Submitted to the 29th International Conference on High-Energy Physics ICHEP98,
Vancouver, Canada, July 1998

Low Q^2 – Intermediate x Structure Function Measurement at HERA

H1 Collaboration

Abstract

The result of a measurement of the proton structure function $F_2(x, Q^2)$ is reported in an extended kinematic domain at low Q^2 ($Q^2 > 0.2$ GeV^2) and intermediate Bjorken-x ($x < 0.0032$) using deep inelastic events with a photon radiation collinear to the incident electron, collected in 1996 by the HERA experiment H1. The rise of F_2 with decreasing x is found to be less steep towards low Q^2 values.

Abstract: 535
Parallel sessions: 4
Plenary sessions: 6

1 Introduction

It has been shown, in previous measurements at HERA ep collider, that the proton structure function F_2 rises rapidly with decreasing x for $Q^2 \geq 1.5$ GeV^2 [1, 2] well described by a pQCD approach, while this rise is much smaller for smaller Q^2 [3, 4] which indicates a transition in a non pertubative regime and can be compared to predictions derived from Regge theory. The measured kinematic domain can be extended at HERA towards high Bjorken x for low values of the squared four-momentum transfer Q^2 making use of deep inelastic events with a photon radiation collinear to the incident electron. Such events can be interpreted as 'non radiative' events produced with a reduced beam energy [5]. This effective reduced center of mass energy allows to reach lower Q^2 and higher x kinematic domain in the detector acceptance. First such structure function measurement have been performed at HERA using 1993 data [6] and improved with higher statistics using 1994 data [1, 7, 8].

In this paper a measurement of F_2 is presented in an extended kinematic domain ($2.2 \cdot 10^{-5} \leq x \leq 0.0032$ and Q^2 $0.2 \leq Q^2 \leq 5$ GeV^2) using such radiative events recorded in 1996 by the H1 detector. The incident electron[1] energy was $E_e = 27.5$ GeV and the proton energy was $E_p = 820$ GeV. The corresponding integrated luminosity of the results presented here is of 4.8 pb^{-1}. The details of this analysis can be found in [9].

2 The H1 Detector

Since the H1 detector is described in details elsewhere [10], only the detectors specific to the measurement of the scattered electron and of the radiated photon, at the basis of this structure function measurement, will be presented here.

The backward lead/scintillating fiber calorimeter, SpaCal, has an angular acceptance of $153^\circ < \theta < 177.8^\circ$. The resolution for electromagnetic clusters is $7.1\%/\sqrt{E(\mathrm{GeV})} \oplus 1.0\%$ [11].

Photons emitted collinearly to the incident electron direction leave the proton beam pipe through an exit widow at $z = -92.3\,\mathrm{m}$ where the proton beam pipe bends upwards. These photons hit the photon detector (PD) of the H1 luminosity system (Fig.1). This detector is located at $z = -102.9\,\mathrm{m}$ on the z axis corresponding to the proton beam. A $2\,X_0$ long lead filter, followed by a $1\,X_0$ long water Čerenkov counter, is located in front of the Photon Detector. The filter protects the photon detector against low energetic synchrotron radiation. The water Čerenkov counter (VC), served primarily as a veto counter (to tag and reject early photon showers), is used in this analysis to provide an estimation of the energy deposited in the lead filter and the VC itself. This energy is combined with the energy measurement in the crystals. The aperture of the photon detector is $\theta_\gamma \leq 0.45\,\mathrm{mrad}$ limited by the inner diameter of the lead collimator in front. The energy resolution is $\sigma(E)/E = 24\%/\sqrt{E(GeV)} + 1\%$. Another part of the H1 luminosity system is the Electron Tagger (ET) which is located beside the electron beam pipe at $z = -33.4\,\mathrm{m}$. It is used in this analysis to identify background events with small angle scattered electrons.

[1] Throughout this paper, both the incident and the scattered positron is referred to as an electron.

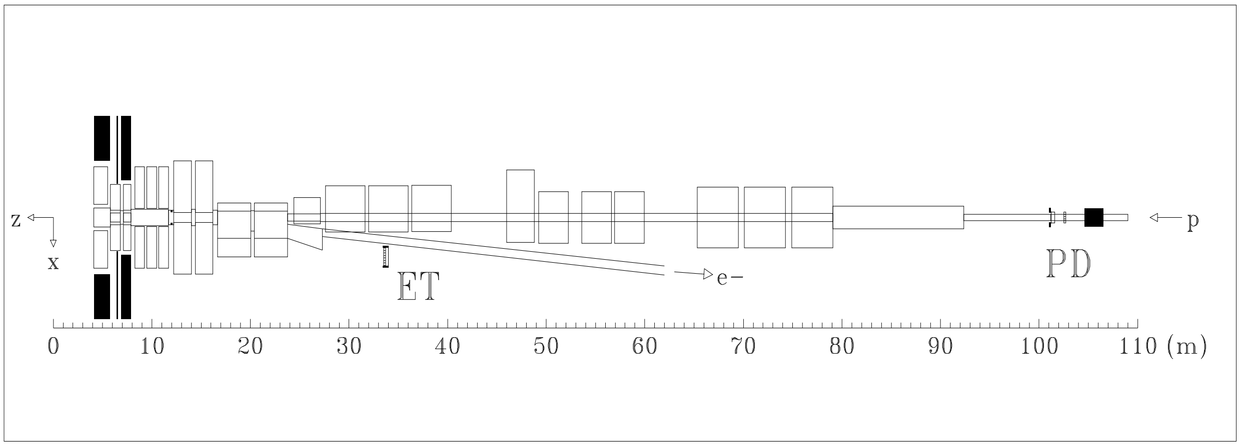

Figure 1: *A schematic view of the H1 luminosity system.*

3 Kinematics

Since all final state particles are detected in the H1 detector (apart from those lost in the beam pipe and neutrinos) including the collinearly radiated photon, it is possible to use different methods to reconstruct the kinematics, combining or not the leptonic and the hadronic final states and including the radiative photon. Our measurement is based on two methods.

- The Electron method (e) makes use only of the scattered electron and the radiative photon:

$$Q_e^2 = 4(E_e^0 - E_\gamma)E_e \cos^2\frac{\theta_e}{2} \qquad y_e = 1 - \frac{E_e}{E_e^0 - E_\gamma}\sin^2\frac{\theta_e}{2} \qquad x_e = \frac{Q_e^2}{y_e\ s^{\mathrm{eff}}}$$

  with the effective center of mass energy $s^{\mathrm{eff}} = 4(E_e^0 - E_\gamma)E_p^0$ varying for each event, where E_e^0, E_γ, E_e, θ_e, and E_p^0 are respectively the electron beam energy, the radiative photon energy, the scattered electron energy and polar angle, and the proton beam energy.

- The Sigma method (Σ) makes use of the scattered electron, the hadronic final state and the radiative photon:

$$y_\Sigma = \frac{\Sigma_h}{\Sigma_h + E_e(1-\cos\theta_e)} \qquad Q_\Sigma^2 = \frac{E_e^2\sin^2\theta_e}{1-y_\Sigma} \qquad x_\Sigma = \frac{Q_\Sigma^2}{y_\Sigma\ s^{\mathrm{eff}}}$$

  where $\Sigma_h = \sum_i^{had}(E_i - p_{z,i})$ is summed over all detected particle of the hadronic final state.

Those two methods are complementary from the resolution and the sensitivity to the radiative corrections.

4 Event Selection

Deep inelastic events with hard photon emission collinear to the incident electron are selected if they satisfy the following criteria:

- the scattered electron, which is defined to be the leading cluster in the SpaCal backward calorimeter, has an energy E_e above 6 GeV and a cluster radius smaller than 3.5 cm. In addition there must be a also track segment in the tracking chamber in front of SpaCal matched to the cluster in the SpaCal within 2 cm along the radial direction. The scattered electron polar angle measurement is determined by this tracking device,

- a photon energy, E_γ, above 7 GeV is required in the Photon Detector, corresponding to the radiative photon candidate,

- a reconstructed event vertex exists, which is determined using the central or forward trackers, within 35 cm of the average event vertex position along the beam (z) direction;

- to reject some background contaminations, there must be no energy in the Electron Tagger and the matching between the total energy in the main detector (i.e. all detectors except the luminosity system) and the Photon Detector is such that:

$$-0.5 < \Delta = \frac{E_\gamma - E_{miss}}{E_\gamma} < 0.5 \quad \text{and} \quad E_{miss} - E_\gamma > -5GeV \tag{1}$$

  where the missing energy $E_{\rm miss} = E_e^o - \frac{1}{2}\sum_i^{all}(E_i - p_{z,i})$, the sum running on all detected particles of the main detector.

5 Monte Carlo Programs

Acceptance corrections and background contributions are studied with the data and with Monte Carlo simulations. Deep inelastic Monte Carlo events containing a radiative photon were generated using DJANGO [12]. This program is based on HERACLES [13] for the electroweak interaction and on LEPTO [14] to simulate the hadronic final state. HERACLES includes complete first order radiative corrections, including the real photon radiation selected here. The photoproduction background was simulated using the PHOJET [15] generator for γp interactions, based on a sample corresponding to the luminosity of the data. The detector response of the Monte Carlo events was simulated in detail and subjected to the same reconstruction and analysis chain as the real data.

6 Background estimate

The remaining background in the selected sample mainly comes from two sources: the overlap of bremsstrahlung events on deep inelastic scattering events, and on photoproduction events.

6.1 Deep Inelastic Background

The first non negligible background source comes from the overlap in the same bunch crossing of a deep inelastic event (2) (which can be radiative or not) and a bremsstrahlung event (3):

$$e^- p \to e^- X \quad , \tag{2}$$

$$e^- p \rightarrow e^- p \gamma \quad . \tag{3}$$

This background contamination is reduced by applying the requirements on the Electron Tagger energy and on the total energy balance applied with the cut on the Δ variable. Indeed for such events, the missing energy in the main detector is expected to be close to zero (the events (2) are almost fully contained in the main detector), and therefore Δ to be close to 1.

This background is simulated by overlapping deep inelastic events (radiative or not) from the DJANGO Monte Carlo with bremsstrahlung events recorded in 1996. To normalise this background, special cuts are applied in order to have a pure background sample in the data on which the simulated sample will be normalised. These cuts correspond to require an energy for the scattered electron candidate above 20 GeV and $\Delta > 0.5$, while no cut is applied on the Electron Tagger. The scattered electron energy, Electron Tagger energy and Δ distributions are shown on Figure 2 after normalisation.

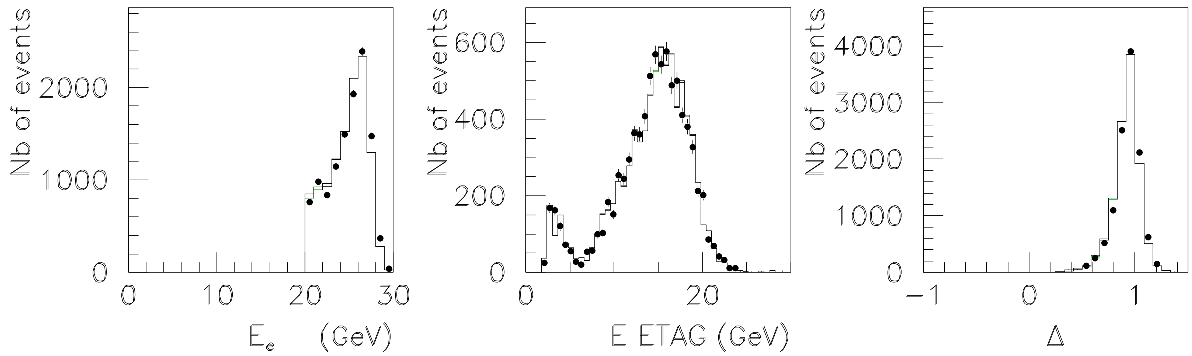

Figure 2: *Scattered electron energy (E_e), Electron Tagger energy (E ETAG) and Δ distributions for the deep inelastic overlapped with bremsstrahlung background normalisation. The histograms correspond to the simulated background and the points to the data.*

6.2 Photoproduction Background

The second main background contribution is due to the photoproduction events, for which a particle of the hadronic final state fakes the electron candidate in the SpaCal, overlapped with a bremsstrahlung event (3).

This background is simulated by overlapping photoproduction events from PHOJET Monte Carlo with bremsstrahlung events recorded independently of the main data sample. To normalise this background, the following cuts are applied in order to have a (almost) pure background sample in the data: the energy of scattered electron candidate must be between 5 and 8 GeV, and the electromagnetic cluster radius, ECRA, must be larger than 3 cm. No cut is applied on the Electron Tagger nor on the Δ variable. The scattered electron energy, Electron Tagger energy and ECRA distributions are shown on Figure 3 after normalisation. In this subsample, a small contribution of the deep inelastic background is observed (black histograms on Figure 3), which has been normalised in an independent way in the previous step. The possible radiative character of the photoproduction events has not been simulated. The nevertheless good description of the global photoproduction background indicates the lack of possible radiative effect on the reconstructed variables.

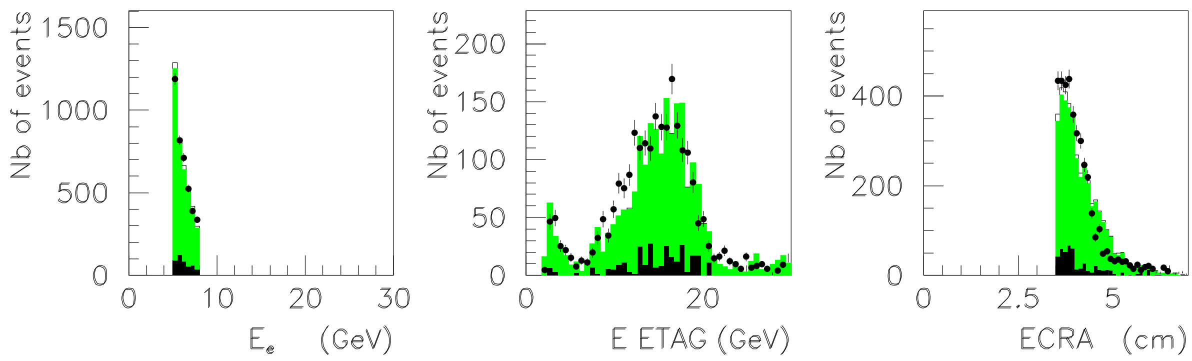

Figure 3: *The energy of the scattered electron candidate (E_e), Electron Tagger energy (E ETAG) and ECRA distributions. The grey histograms represent the photoproduction overlapped with bremsstrahlung background, the black histograms are the deep inelastic overlapped with bremsstrahlung background and the points are the data.*

7 Results

7.1 Data - Monte Carlo Comparison

The selected data are compared to the DJANGO simulation of radiative deep inelastic events to which the simulated backgrounds are added. The input structure function used in the Monte Carlo is the parameterisation ALLM97 [16]. The Figure 4 shows the data and simulation comparison, normalised to the luminosity for the scattered electron energy and polar angle, the radiative photon energy, the Σ_h variable and the Δ variable. The kinematic variables x, Q^2 and y for both electron and Sigma methods are presented on Figure 5. Note that due to the SpaCal trigger structure and some local inefficiencies, the cluster position in the transverse plane has a complicated mapping which gives a irregular shape to the scattered electron polar angle distribution. The distribution in the (x, Q^2) plane is shown in Figure 6 along with the bins used for the F_2 measurement.

7.2 Radiative Corrections

The DJANGO program includes the complete first order of radiative corrections (order α^3) but no order beyond. The measurement being based on events at the order α^3, no radiative correction are so far included. Some recent calculations in the specific case of a radiative tagged photon [17] including for the first time NLO terms, allow us to compute for each bin center the radiative correction for the Electron method, using the MISICA program. The correction is estimate to be up to 20% at the highest y values with a 5% uncertainty. In its present version this program only allows radiative corrections to be computed for the Electron method. The effect for the Sigma method is expected to be smaller and will be included in the future. A global 5% uncertainty has been quote to cover this effect.

7.3 F_2 Extraction

In the Q^2 range of the present analysis and with an initial radiative photon collinear to the incident electron beam of energy above a few 100 MeV, the differential cross section in x and Q^2 is given

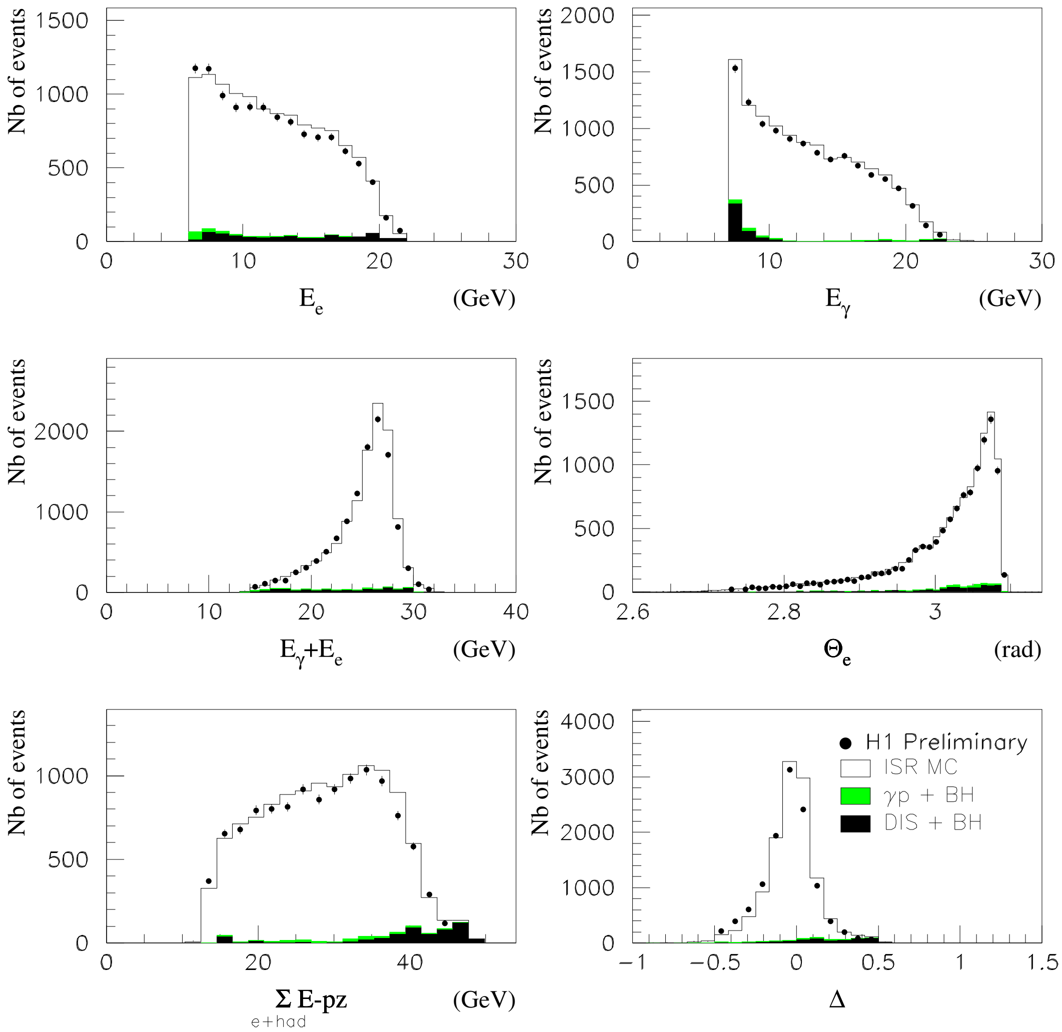

Figure 4: *Scattered electron energy (E_e), radiative photon energy (E_γ), sum of energies of the electron and the photon ($E_e + E_\gamma$), electron polar angle (Θ_e), the Σ_h variable and Δ distribution. The empty histograms correspond to the Monte Carlo of the radiative events, black histograms are the deep inelastic background, grey histograms are the photoproduction background and the points are the data.*

by [5]

$$\frac{\mathrm{d}^2\sigma}{\mathrm{d}x\mathrm{d}Q^2} = \int_0^{z_1} \mathrm{d}z \frac{\mathrm{d}^3\sigma}{\mathrm{d}x\mathrm{d}Q^2\mathrm{d}z} = \int_0^{z_1} \mathrm{d}z \frac{\alpha^3}{xQ^4} P(z) \left[2(1-y) + \frac{y^2}{1+R}\right] F_2(x, Q^2)(1+\delta_{ho}) \tag{4}$$

with

$$z = \frac{E_e^0 - E_\gamma}{E_e^0} \qquad \text{and} \qquad P(z) = \frac{1+z^2}{1-z} \ln \frac{{E_e^0}^2 \theta_a^2}{m_e^2} - \frac{2z}{1-z} \tag{5}$$

where R is related to the longitudinal structure function, F_L, by $R = F_L/(F_2 - F_L)$, here assumed to be $R = 0$. The integration over z is done for $z_1 = 0.74$ corresponding to $E_\gamma > 7$ GeV and on the photon detector acceptance $\theta_a \simeq 0.45$ mrad. The term δ_{ho} stands for the higher order

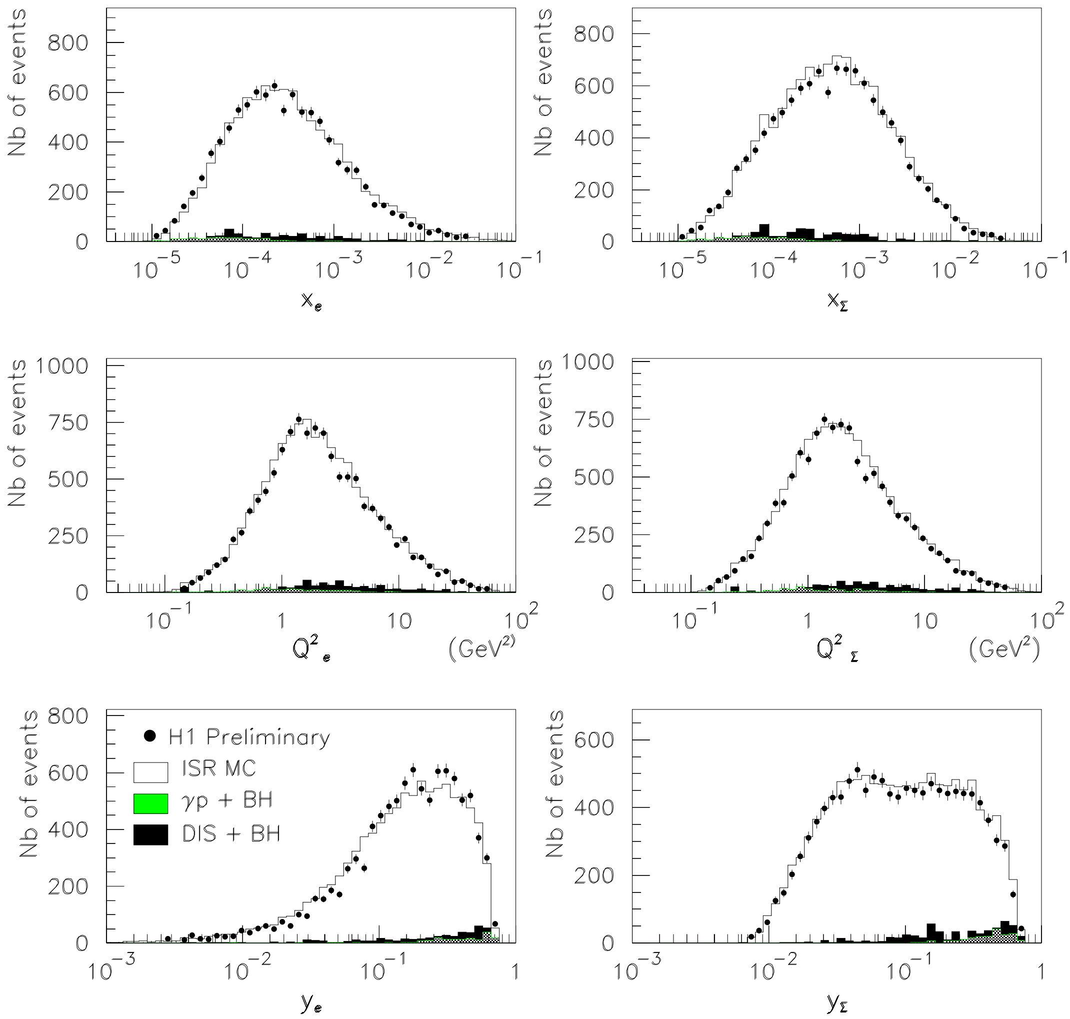

Figure 5: *Kinematic variables x, Q^2 and y for both electron (e) and Sigma (Σ) methods. Same histogram definition as previous Figure.*

radiative correction.

The acceptance and efficiency corrections are based on simulations and on studies using independent detectors (in particular for the trigger efficiencies). For each bin the purity and the stability [2] have been estimated on a Monte Carlo basis, and required to be above 30%. Comparing the two methods, the Sigma method shows higher purity and stability everywhere in the kinematic region except at low x values. Therefore the Sigma method is used except for the lowest x bin for each Q^2 bin.

Additional systematic errors have been estimated in each bin by varying the analysis procedure. The dominant errors come from the uncertainty on the radiative photon energy scale, its

[2] The purity is the ratio, in a given bin, of the number of events generated and reconstructed over the number of events generated. The stability is the ratio of the number of events generated and reconstructed over the number of events reconstructed.

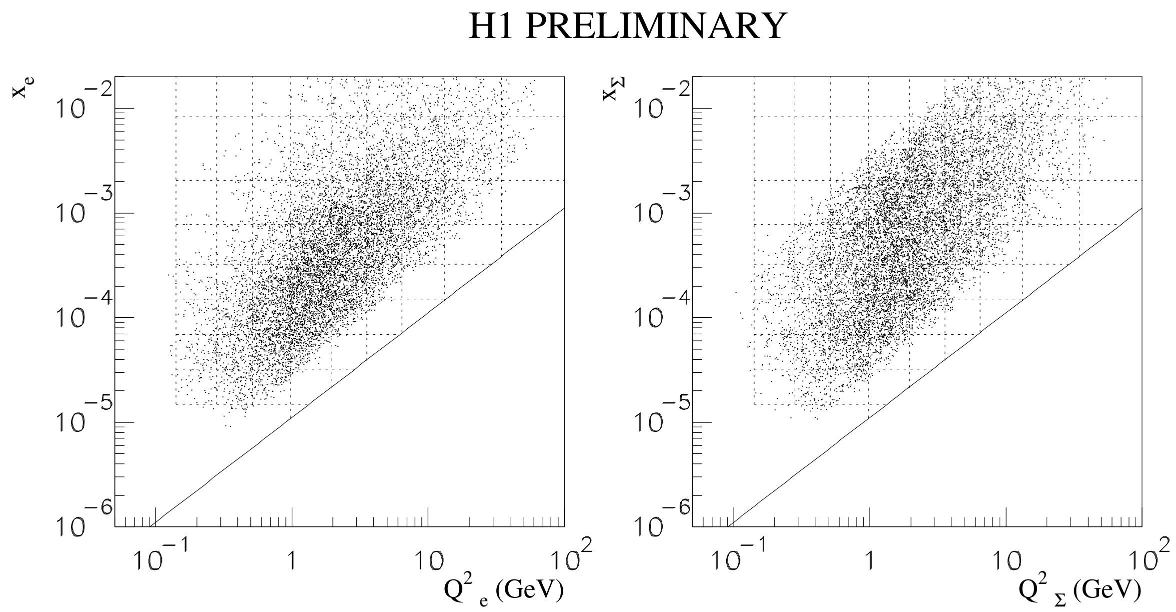

Figure 6: *Distribution in the* (x, Q^2) *plane for the Electron method (a) and the Sigma method (b). The binning is shown in overlay.*

variation between 2% at 7 GeV decreasing linearly to 1% at 20 GeV leads to a typical uncertainty of 5%, up to 10% at higher x and low Q^2. A systematic error on electron energy scale of 5% at 6 GeV to 2% at 20 GeV leads to a typical uncertainty of 10% up to 25% at the lowest Q^2 values. The vertex reconstruction efficiency brings an uncertainty up to 15% at the lowest y decreasing to 3% for $y > 0.03$. The resulting error estimate on F_2 measurement is typically 10%.

The preliminary F_2 values are shown in Figure 7 as a function of x for different Q^2 values between 0.2 and 5. GeV ^{2}. The measured points are compared to the ALLM97 [16] and to the GRV(94) [18] parameterisation.

The measurement presented here extends the previous HERA measurements in the transition region between photoproduction and deep inelastic scattering, down to $Q^2 = 0.2$ GeV ^{2} and towards large x at larger Q^2 values. The measurement is in agreement in the previously covered kinematic region with the previous HERA results.

8 Conclusion

A measurement of the F_2 proton structure function has been performed in an extended kinematic domain towards low Q^2 ($Q^2 \geq 0.2\,\text{GeV}^2$) and towards higher x ($x \leq 0.0032$) using deep inelastic events containing a hard photon radiation collinear to the electron beam. The rise of F_2 with deceasing x is found to be less steep towards low Q^2 values. The measurement is in agreement with previous structure function measurements at HERA where there is overlap of the kinematic ranges of measurement and with the prediction based on a phenomenological approach to the transition region between photoproduction and deep-inelastic ep scattering.

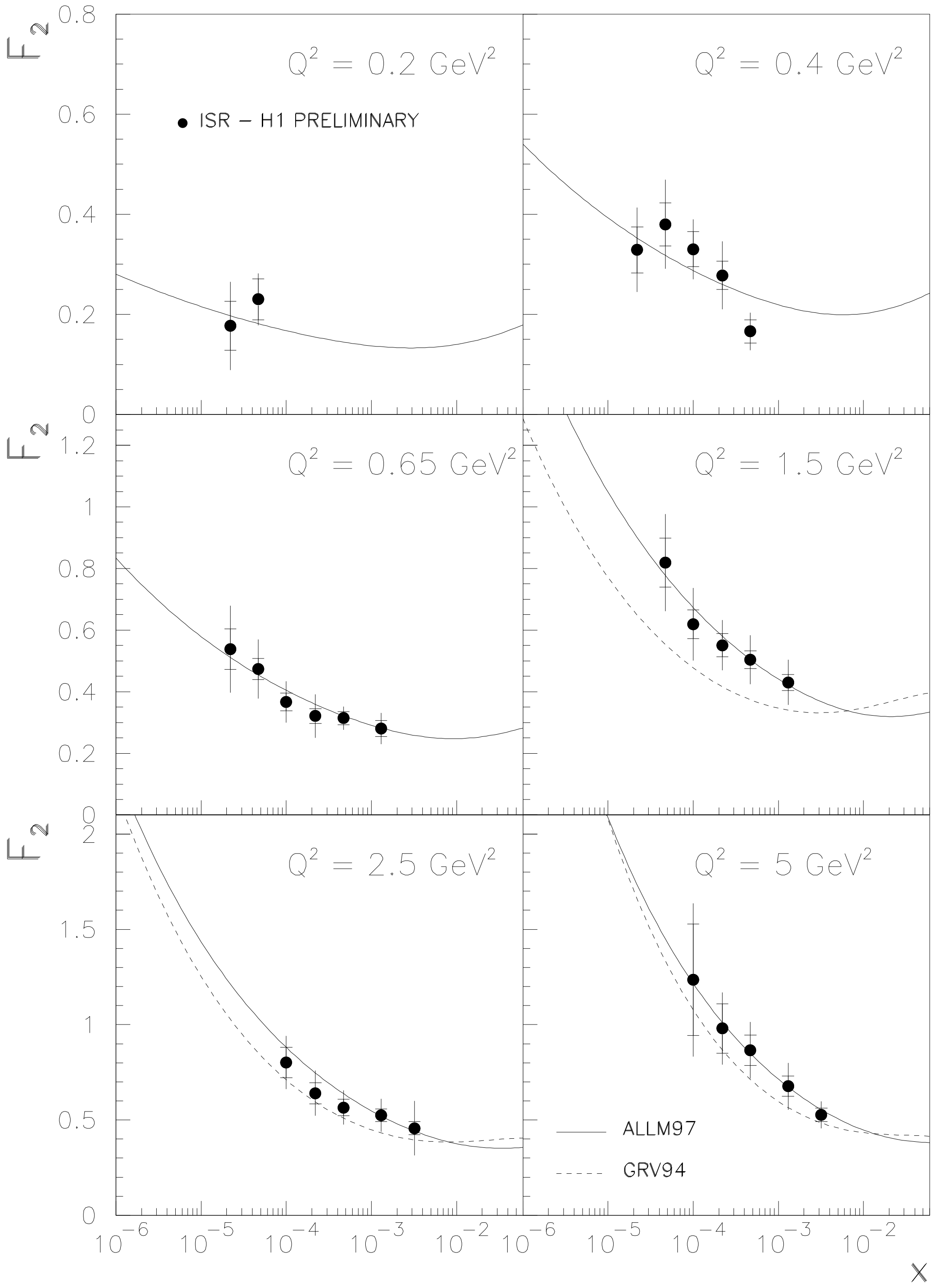

Figure 7: *F_2 values in of x for different Q^2 values. The inner error bar shows the statistical error and the outer the total error (quadratic sum of statistic and systematic). The parameterisations ALLM97 and GRV(94) (above 1. GeV^2) are also shown.*

References

[1] H1 Collab., S. Aid et al., *Nucl. Phys.* B **470**, 3-38 (1996).

[2] ZEUS Collab., M. Derrick et al., *Z. Phys.* C **72**, 399-424 (1996).

[3] H1 Collab., Adloff et al., *Nucl. Phys.* B **497**, 3-28 (1997).

[4] ZEUS Collab., J. Breitweg et al.,*Phys. Lett.* B **407**, 432-448 (1997).

[5] M.W. Krasny et al., *Z. Phys.* C **53**, 687 (1992).

[6] L. Favart, PhD thesis, Université Libre de Bruxelles, Nov. 1995.

[7] M. Hütte, PhD thesis, Universität Dortmund, Dec. 1996.

[8] A. Frey, PhD thesis, Universität Bonn, Feb. 1996,
ZEUS Collab.,M. Derrick et al., *Z. Phys.* C **69**, 607-620 (1996).

[9] S. Schleif, PhD thesis, in litt.

[10] H1 Collab., I. Abt et al., *Nucl. Instrum. Methods* A **386**, 310 (1997) and **A386**,348 (1997).

[11] H1 SPACAL group, R.D. Appuhn et al., *Nucl. Instrum. Methods* A **374**, 149-156 (1996).

[12] G. A. Schuler and H. Spiesberger, Proceedings of the Workshop Physics at HERA, Vol. 3, eds. W. Buchmüller and G. Ingelman, DESY (1992) p. 1419.

[13] A. Kwiatkowski, H. Spiesberger and H.-J. Möhring. Comp. Phys. Comm. 69 (1992) 155.

[14] G. Ingelman, Proceedings of the Workshop Physics at HERA, Vol. 3, eds. W. Buchmüller and G. Ingelman, DESY (1992) p. 1366.

[15] R. Engel and J. Ranft, *Phys. Rev.* D **54**, 4244 (1996).

[16] H. Abramowicz, E. Levin, A. Levy, U. Maor, *Phys. Lett.* B **269**, 465 (1991) and an update in hep-ph/9712415.

[17] H. Anlauf, MISICA program, private communication and hep-ph/9711333.

[18] M. Glück, E. Reya and A. Vogt, *Z. Phys.* C **67**, 433 (1995).